Influence of iridium oxide loadings on the performance of PEM water electrolysis cells: Part I–Pure IrO2-based anodes

Caroline Rozain, Eric Mayousse, Nicolas Guillet, Pierre Millet

Influence of iridium oxide loadings on the performance of PEM water electrolysis cells: Part I – Pure IrO_2-based anodes

Caroline Rozain[a], Eric Mayousse[a], Nicolas Guillet[a*], Pierre Millet[b]

[a]Univ. Grenoble Alpes, F-38000 Grenoble, France
CEA, LITEN F-38054Grenoble, France

[b]Institut de Chimie Moléculaire et des Matériaux d'Orsay, Université Paris-Sud 11, Orsay, France

∗ Corresponding author. Tel.: +33 479 792 178. E-mail address: nicolas.guillet@cea.fr

Abstract

The influence of iridium oxide loadings at the anode of PEM water electrolysis cells on the overall electrochemical performance was studied using cyclic voltamperometry and electrochemical impedance spectroscopy, and by measuring polarization curves at 80°C. Membrane electrode assemblies with reduced metal loadings (0.25 mg cm^{-2} of Pt at the cathode and 0.5 mg cm^{-2} of IrO_2 at the anode) were prepared using the decal method. A typical cell voltage of 1.72 V was recorded using a 25 cm^2 cell with a Nafion® 115 membrane at a current density of 1 A cm^{-2} (at 80°C and atmospheric pressure). Performances measured with such reduced noble metal loadings are similar to those obtained with conventional loadings of several mg cm^{-2}.

Keywords: water electrolysis, PEM, iridium oxide, low catalyst loading.

Graphical abstract

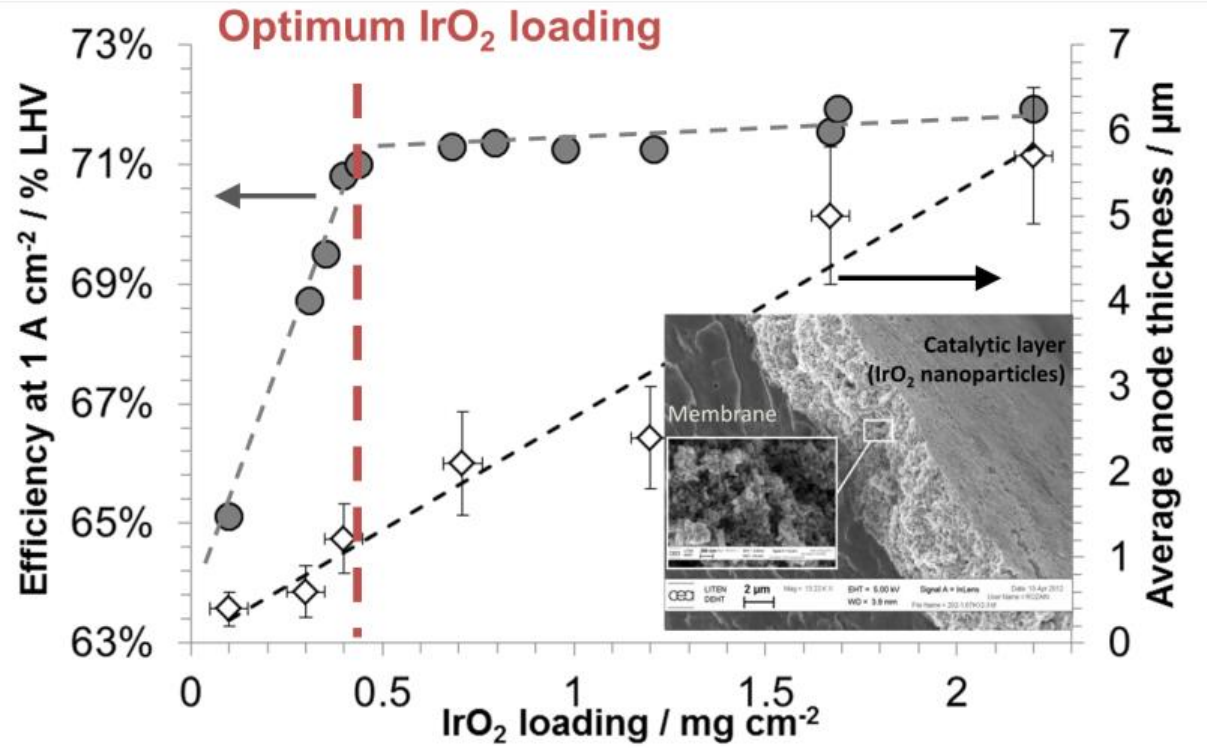

Highlights

- The role of the anodic catalyst loading (IrO_2 nanoparticles) on the performances of PEM water electrolysis cells was studied.
- A model was developed and used to fit the experimental plots of voltammetric charge *vs.* catalyst loading.
- An optimal catalyst loading of 0.5 mg_{IrO2} cm^{-2} was determined.

List of symbols

A, dimensionless number	Fitting parameter
B, C m^{-2}	Fitting parameter, capacity of a single layer of catalyst
η_{HHV}, %	Efficiency, referred to the “Higher Heating Value” of hydrogen (286 kJ mol^{-1}), considering that the latent heat of vaporization of water in the combustion products can be recovered.
η_{LHV}, %	Efficiency, referred to the “Lower Heating Value” of hydrogen (244 kJ mol^{-1}), considering thatthe latent heat of vaporization of water is not recovered.
m_{IrO2}, mg cm^{-2}	IrO_2 loading at the anode
m_{layer}, g	Mass of a single layer of catalyst particles
n	Number of catalyst single layers in the electrode
N	Total number of catalyst single layers in the electrode
q, C cm^2	Voltammetric charge
Q*, C cm^{-2}	Total coulombic charge accessible at the electrode
Q_{inner}, C cm^{-2}	Inner coulombic charge, $Q_{inner} = Q^* - Q_{outer}$
Q_{outer}, C cm^{-2}	Outer coulombic charge
R, nm	Radius of spherical catalyst particle
ρ, g cm^{-3}	IrO_2 volumetric weight (11.66 g cm^{-3})
RHE, V	Reversible Hydrogen Electrode
ν, mV s^{-1}	Electrode potential scan rate

1. Introduction

The massive utilization of fossil fuels - and the associated negative impact on the environment - are calling for the development and implementation of clean, efficient and carbon-free energy carriers such as molecular hydrogen. Among other processes, proton exchange membrane (PEM) water electrolysis is considered as one of the key technologies that can be powered by renewable energy sources and can be used for the large-scale production of clean hydrogen [1]. Because of the high acidity of the perfluorinated membrane materials used in state-of-the-art PEM water electrolysis (PEMWE) cells, expensive noble metals or their oxides (platinum for the hydrogen evolution reaction or HER at the cathode and iridium for the oxygen evolution reaction or OER at the anode) are required as electrocatalysts. At the cathode, significant progresses made in polymer electrolyte membrane fuel cell (PEMFC) technology led to the reduction of platinum loadings down to 0.3 mg cm^{-2}. This was achieved by using high surface area carbonaceous catalyst supports such as carbon powders [2], carbon nanofibers [3], and even carbon nanotubes [4,5]. Pt/C catalysts used in PEMFC cells can also be used at the cathode of PEMWE cells. At the anode, the OER takes place at high potential (≈ 1.5-1.8 V *vs.* RHE), a situation that proscribes the use of carbon-based materials as catalyst support (carbon is oxidized according to the reaction $C + 2H_2O \rightarrow CO_2 + 4H^+ + 4e^-$ at a potential of only +0.206 V *vs*. RHE [6,7]). Consequently, high loadings of unsupported iridium oxide (2-4 mg cm^{-2}) are generally used [8]. In order to reduce the capital expense of PEMWE cells, there is a need to reduce IrO_2 contents. A reduction of the IrO_2 loading can be achieved by either supporting the IrO_2 particles on a conducting support material (titanium carbide [9,10], tantalum carbide [10,11] and doped or reduced form of titanium [12,13] or tin oxide [14] have been reported in the literature) or by incorporating some inexpensive and electrochemically inert materials such as TiO_2 [15,16], SnO_2 [17–20], indium or antimony – tin oxide [21–24] or Ta_xO_2 [25] to the catalyst layer in order to form Ir-based mixed oxides. However, along with the instability of most of those supports in oxidizing environment [26], the IrO_2 loadings on these electrodes are still quite high (1.5 to 2 mg cm^{-2}).

Another approach is to reduce the IrO_2 loading. To the best of our knowledge, only few studies have been made to determine the effect of a reduction of the catalyst loading at the anode of PEMWE cells [9, 27–30]. For example, Ma *et al.* were able to reduce the catalyst loading down to 1 mg cm^{-2} IrO_2 but this led to a significant reduction of cell performances [9]. The problem is still unsolved and therefore, the objective of the research work reported here was to investigate in detail the influence of IrO_2 loading on the overall performance of PEMWE cells and to optimize the structure of catalytic layers.

2. Experimental

2.1 MEA preparation

A Nafion® NRE 115 CS (DuPont™) membrane (127 µm thick) was used as solid polymer electrolyte. Commercial iridium dioxide (Surepure® Chemetals) and 46 *wt.*% Pt/carbon black (TEC10V50E, Tanaka® Kikinzoku Int.) powders were respectively used as oxygen and hydrogen evolution electrocatalysts. The amounts of catalyst powder and Nafion® ionomer (5 *wt.* % in water and ethanol, D520 DuPont™) were accurately weighed and then ultrasonically dispersed in a mixture of deionized water and isopropanol (volume ratio 1:1). The ionomer content of the electrocatalytic layers at the anode and the cathode was set to 10 and 26 *wt.*% respectively. Membrane – electrodes assemblies (MEAs) were prepared by coating these suspensions onto the membranes. In principle, several methods can be used to coat the anodic and cathodic catalyst layers on each side of the proton exchange membrane [31,32]. For the preparation of small surface MEAs, spray coating is usually preferred [9,27,29]. However, for larger MEAs (typically hundreds of cm² or more), blade coating or screen printing is more appropriate, due to the speed of the process, its reliability and the homogeneity of the coatings thus obtained. Whatever the deposition method is, it is often difficult to set and measure accurately the catalyst loadings. This would require a strict control of the atmosphere in contact with the membrane during the process (solvent partial pressure, air moisture, etc.), even when fully dried membranes are used. After many attempts, we found that the decal method was the most appropriate way to prepare batches of MEAs with reproducible catalyst loadings in terms of content and homogenity. MEAs were thus prepared as follows. Catalytic inks (suspensions of catalyst powder and ionomer solutions in solvents) were first sprayed over flat PTFE sheets used as intermediate support. Then the catalyst layer-coated PTFE sheets containing either Pt (cathode) or IrO_2 (anode) were dried at 80°C for 30 minutes in an oven, and circular samples (5.64 cm diameter, ≈ 25 cm^2) were cut by a laser beam and precisely weighed. The membrane was then sandwiched between two catalyst coated decals (one cathode and one anode) and catalysts layers were transferred and bonded onto each side of the membrane by hot pressing at 4 MPa and 135°C for 6 min. After cooling, the decals were peeled away, leaving the two thin layers of catalyst on each side of the membrane. Each PTFE sheet was weighed again after peeling and the difference of weight was used to determine accurately the catalyst loadings transferred to each side of the membrane. For all the experiments reported in this paper, the cathode catalyst loading was kept constant at 0.25 ± 0.05 mg_{Pt} cm^{-2}.

After preparation, MEAs were treated for 1 h in 0.5 M sulfuric acid aqueous solution to remove any impurity and completely exchange the membrane with protons. Then, they were stored in

deionized water (18.2 MΩ cm^{-1}) for 12 h. They were then used for electrochemical characterization using an electrolysis cell. MEAs were clamped between two machined Ti grade 2 monopolar plates. A porous titanium disc made of sintered powder (Applied Porous Technology Co., Sweden, mean pore size value ≈ 10 µm) was used in the anode compartment and a carbon – based gas diffusion layer (SGL group, Sigracet®-34BC) in the cathode compartment. The cell was finally tightened between two stainless steel clamping plates using a dynamometric wrench at to 8 N m.

2.2 Measurement of PEMWE performance

Anodes containing various IrO_2 loadings (ranging from 0.1 to 2.6 mg cm^{-2} IrO_2) were investigated by cyclic voltamperometry, electrochemical impedance spectroscopy (EIS) and by measuring polarization curves. A total of thirteen MEAs were prepared and tested. All parameters (temperature, ionomer content, cathode and membrane) were the same except the anodic catalyst loading.

Electrolysis performances were measured at 80°C and at atmospheric pressure using a 25 cm^2 single cell. Deionized water circulating through the anodic compartment was kept at the same temperature as that of the cell. During experiments, the anode was supplied with deionized water at a constant flow rate of 200 ml h^{-1}. Electrodes were first activated for approximately 12 h, a period during which four polarization curves were recorded in the 0.4-2 A cm^{-2}range using 0.2 A cm^{-2} steps. After activation, stationary polarization curves were recorded from 0.04 to 2 A cm^{-2} by applying a series of current density steps (0.04 , 0.08, 0.12, 0.16, 0.20, 0.40, 0.60, 1, 1.4, 1.8, 2 A cm^{-2}) with a 10 minutes long stabilization period between each step.

EIS experiments were carried out using a high current potentiostat (Bio-Logic Science Instruments SAS, HCP-803, 80 A) at frequencies ranging from 10 kHz down to 200 mHz. Applied current densities were the same than those used for the polarization curves. A stabilization period of 2 min was applied between each step in order to reach a quasi-stationary regime. The amplitude of the sinus current perturbation was carefully chosen for each current to fulfill the linearity conditions of the system, while ensuring a sufficient signal/noise ratio. Purely ohmic resistances were determined by taking high frequency intercepts of Nyquist plots with the real axis, assuming that pure resistance values are obtained at zero phase values. Polarization resistances were taken as the difference between the extrapolated low frequency intercept and the high frequency intercept on the real axis. Impedance data were fitted using the Ec-lab® software.

Coulombic charges associated with the electrochemically active surface area (ECSA) were determined by cyclic voltamperometry at room temperature using a VSP2 Bio-Logic potentiostat before and after polarization experiments. Anodic electrodes (IrO_2) were used as working electrode. A nitrogen-saturated water flow (200 mL h^{-1}) was pumped through the anodic compartment during the measurements. A pure hydrogen atmosphere was set at the cathode (Pt/C) which was used as both counter and reference electrode. Since current densities recorded during cyclic voltamperometry (few tenth of mA cm^{-2}) are small compared to those reached during PEMWE experiments (up to 2 A cm^{-2} during electrolysis), the Pt/C electrode was assumed to behave as a reversible hydrogen electrode (RHE:H_2/Pt, at room temperature and atmospheric pressure) of constant potential, independent of current density passing through. Cyclic voltammograms (CVs) were recorded at different scan rates (from 5 to 100 mV s^{-1}) over a potential domain ranging from the hydrogen to the oxygen evolution reactions (*i.e.* 0.05 V – 1.3 V).

2.3 Physical characterizations

Post-mortem characterization of MEAs with various IrO_2 loadings was carried out by scanning electron microscopy (SEM) analysis. Cross sections of the MEA were prepared by cryofracture and observed with a LEO 1530 field emission gun-scanning electron microscope (FEG-SEM) at an accelerating voltage of 5 kV under a high vacuum. The surface area of the iridium oxide powder was measured by adsorption of liquid nitrogen on the sample with a Beckman Coulter SA3100. The analysis of the isotherms provided the Brunauer-Emmet-Teller (BET) specific surface area. Outgasing was realized at 300 °C during 4 h.

3. Results and discussion

3.1 Anode morphology

Typical SEM images of cryofractured MEAs obtained after electrochemical testing are shown in Figure1. The anodic catalytic layers were found to be several micrometers thick. The mean size of IrO_2 catalyst particles was found to be approximately 15 nm. The specific surface area of the catalyst powder was measured by BET analysis and was estimated to be 35 $m^2\ g^{-1}$.

(a)

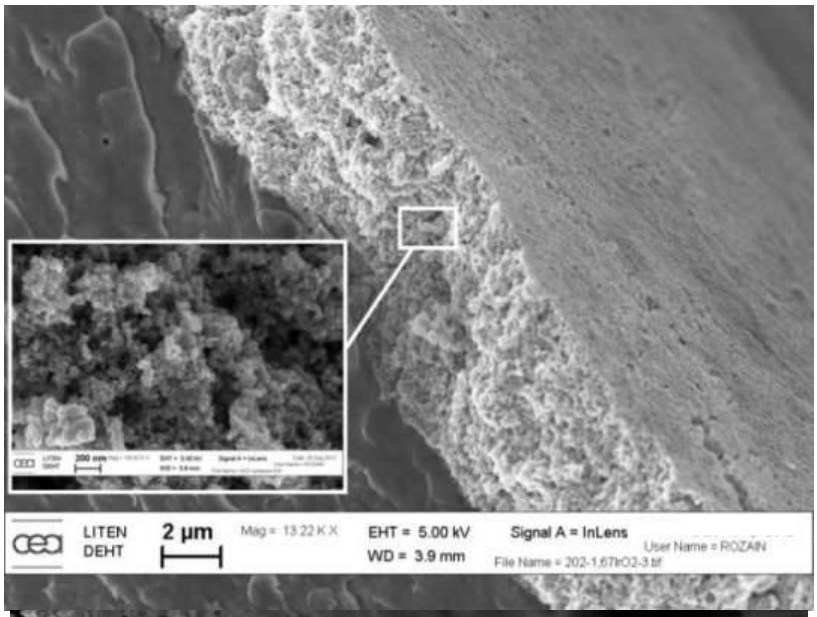

(b)

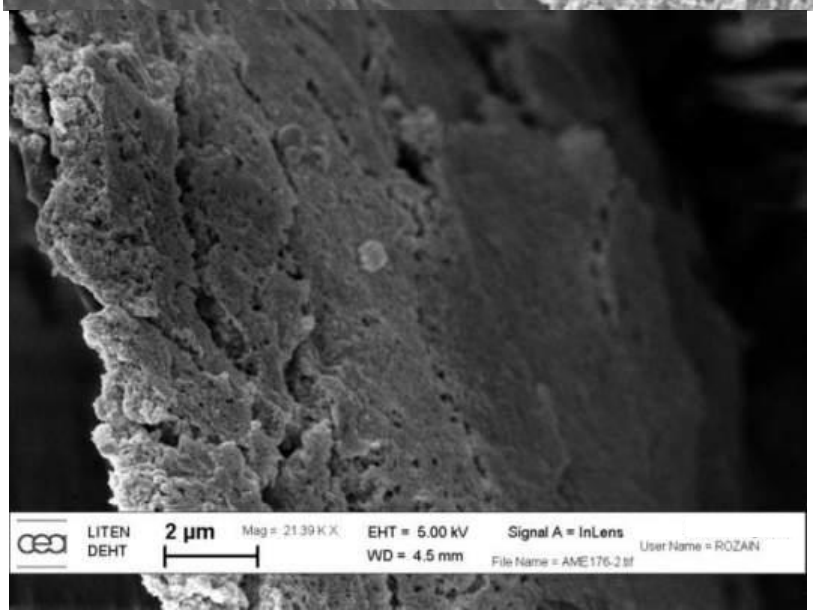

Figure1: SEM images of two anodes with different anodic loadings.

(a) 1.7 mg cm^{-2} and (b) 0.31 mg cm^{-2} IrO_2.

MEAs with high IrO_2 loading show catalytic layers of homogeneous thickness (Figure1-a). MEAs with lower catalyst loadings present cracks and large thickness heterogeneities (Figure1-b).

Figure 2 shows that there is a direct correlation between the anode thickness and the catalyst loading. It should be noted that anode thicknesses was measured only after electrochemical experiments. Since cryofracture is a destructive method and since MEAs are firmly clamped between porous current collectors during cell testing, this may cause the deformation of the active layer. This partly explains the scattering of data observed in Figure 2 although loadings are accurately known.

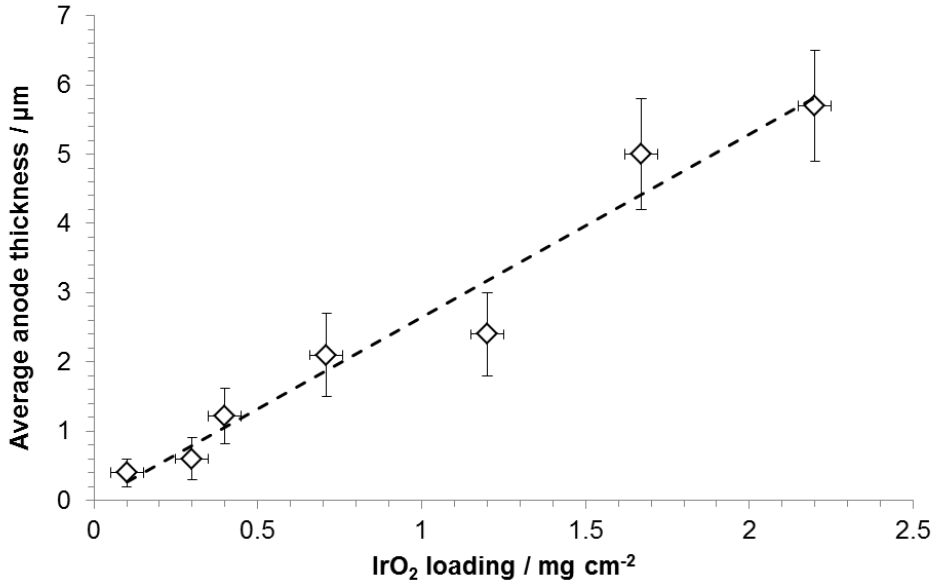

Figure 2: Anode average thickness determined by SEM analysis on cryofractured MEAs as a function of IrO_2 loading.

3.2 Influence of IrO_2 loadings on the electrochemical active surface area of anodes

The number of electroactive sites available for the OER at an oxide surface is generally determined by cyclic voltamperometry. The underlying assumption is that the number of sites probed by this technique is the same than those involved in the OER mechanism. CVs recorded at a constant scan rate of 20 mV s^{-1} on anodes containing various IrO_2 contents, are plotted in Figure 3.

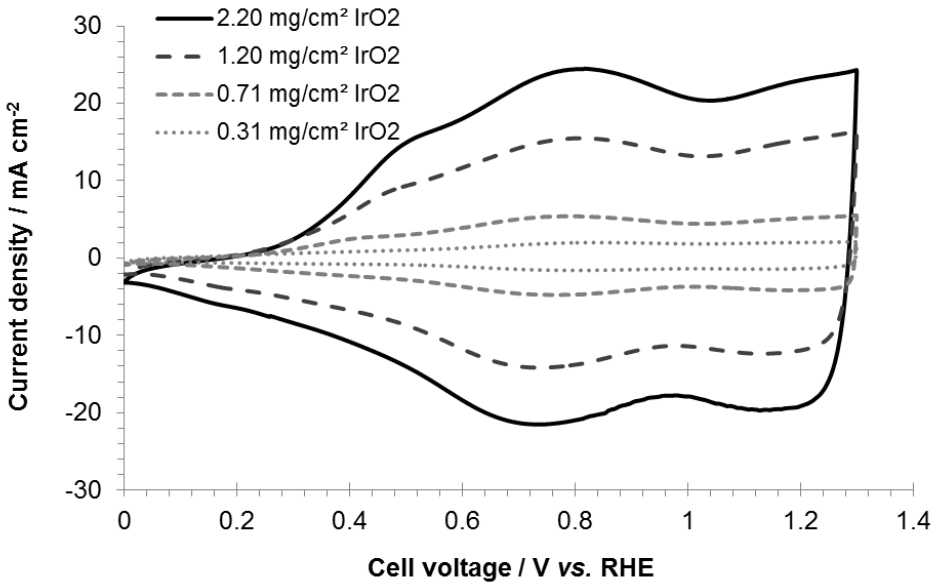

Figure 3: Cyclic voltammograms of anodes with various IrO_2 loadings at a sweep rate of 20 mV s^{-1} and room temperature.

These CVs are all characteristic of IrO_2 catalysts, as previously reported [33]. Their shape is characterized by the presence of two broad peaks corresponding to the solid state redox transitions that occur due to the adsorption and oxidation of oxygenated species from the electrolyte [34]. Iridium dioxide is reversibly oxidized and reduced through a mechanism that involves a proton transfer to/from the surrounding electrolyte [35,36], as follows:

$$IrO_a(OH)_b + \delta H^+ + \delta e^- \leftrightarrows IrO_{a-\delta}(OH)_{b+\delta} \qquad \text{Equation 1}$$

Active surface areas were evaluated for each anode according to the method proposed by Ardizzone *et al.* [36] and Lodi *et al.* [37]. The surface area under the anodic voltammetric curves (

Figure 3) represents a voltammetric charge (q) which is proportional to the true surface area of the electrode-polymer interface [36]. This charge was determined by direct integration of experimental curves. It can be observed (Figure 4-a) that (q) decreases as the potential scan

rate (ν) is increased. Assuming that the scan rate dependence of q is relative to the diffusion of protons to the surface, q is supposed to vary linearly versus $\nu^{-1/2}$. Figure4-a shows that the linearity is quite well observed for IrO_2 catalyst loadings up to 2.2 mg cm^{-2}.

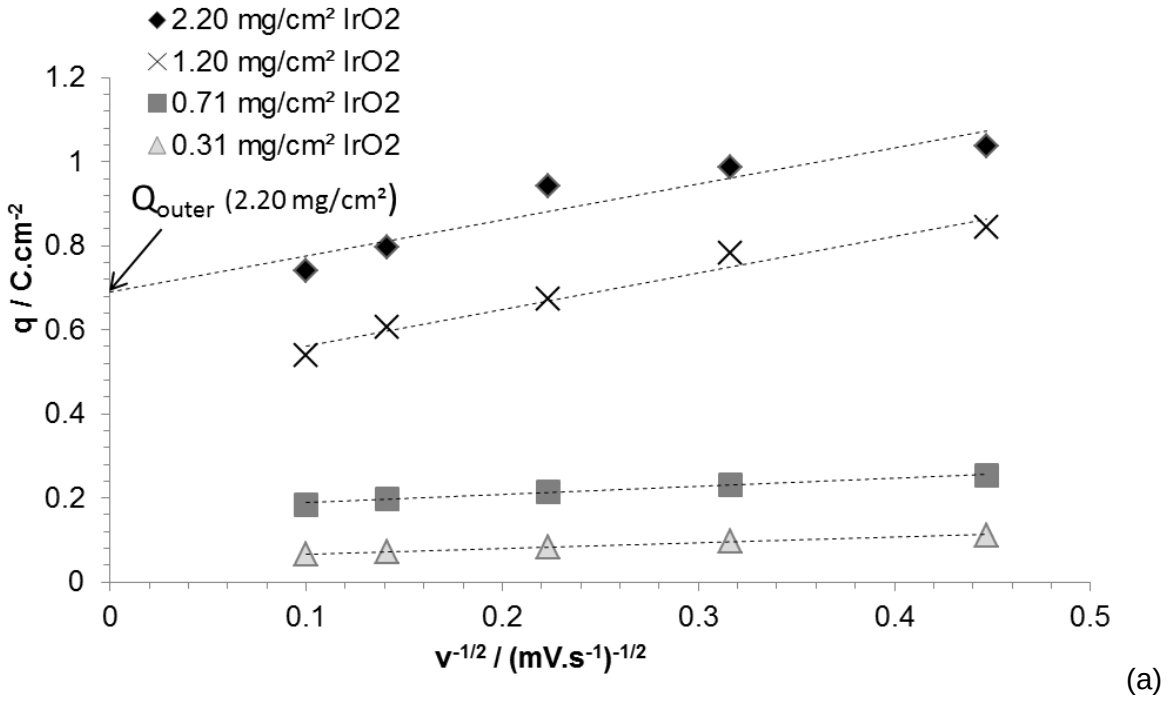

(a)

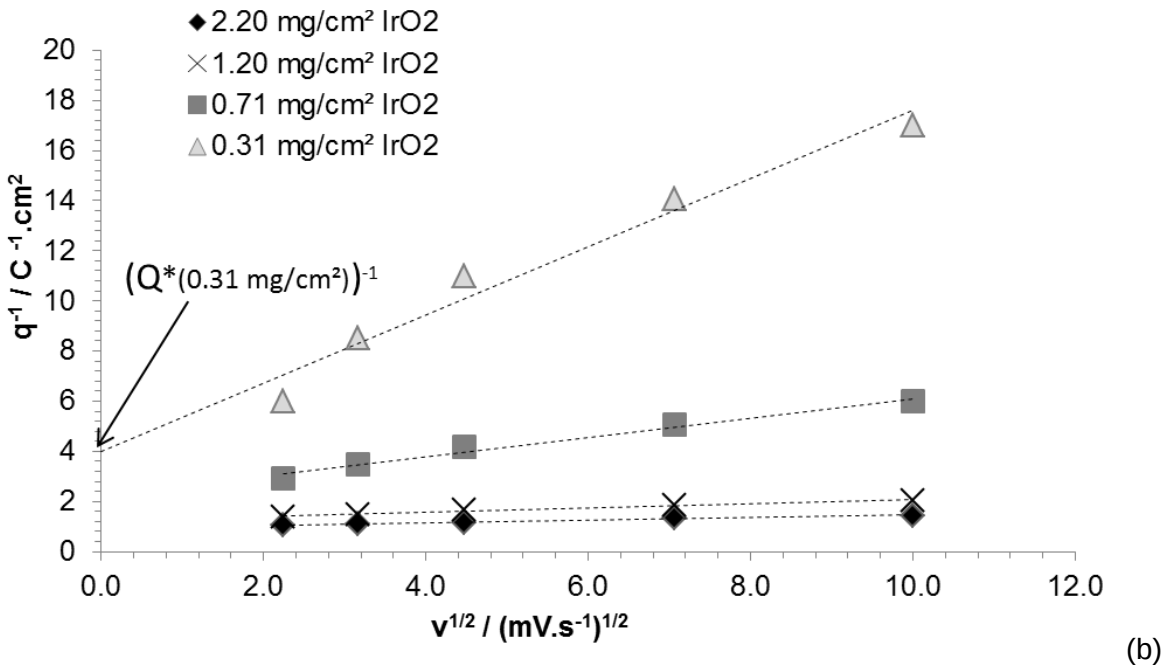

(b)

Figure4: Dependence of voltammetric charge (q) of anodes on scan rates for different catalyst loading

a- q *vs.* $\nu^{-1/2}$ plot for different loadings. Extrapolation of the linear section to $\nu = \infty$ (y intercept) is used to determine Q outer.

b- q^{-1} *vs.* $\nu^{1/2}$ plot for different loadings. Extrapolation of the linear section to $\nu = 0$ (y intercept) allows the determination of $(Q^*)^{-1}$.

Extrapolation of the linear sections to the origin gives the charge values at $\nu=\infty$. These charge values are related to the number of catalytic sites available at the surface of catalyst particles (*i.e.* in direct contact with the electrolyte). This is called the "outer" surface of the oxide (Q outer). On the other hand, a plot of q^{-1} versus $\nu^{1/2}$ linearly extrapolated to $\nu=0$ (Figure 4-b) provides a measure of the entire charge (Q*) accessible at the catalyst surface. The total charge Q* is assumed to be the sum of the inner (Q inner) and outer (Q outer) charges: Q* = Qinner + Qouter. The inner charge is related to the existence of less accessible surface regions (those located at loose grain boundaries, in pores, cracks, etc.).

The voltammetric charge (Q*) can be considered as an indirect measure of the number of electroactive sites (the real electrochemical surface area or ESCA) of the electrode even though a conversion of this charge into a measure of the surface area is a difficult task because the nature of the surface reactions is not precisely known [36]. Hence, the following discussion is based on the values of the total charge (Q*). Figure 5 shows a plot of Q* versus the catalyst loading. The voltammetric charge increases logically with the IrO_2 loading. For catalyst loadings less than 1 mg cm^{-2}, i.e. for thin electrodes (less than 3 µm thick), Q* increases linearly with the catalyst loading. For catalyst loadings larger than 2 mg cm^{-2} (layers thicker than 5 µm), Q* tends to reach a constant value close to 1 C cm^{-2}. According to these results, the optimal loading is in the 1.5 - 2 mg cm^{-2} range.

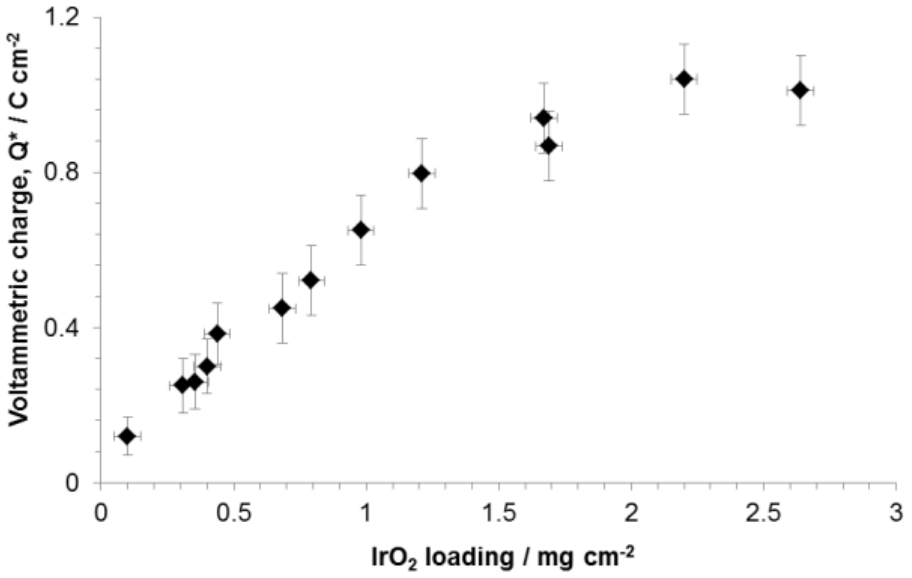

Figure 5: Evolution of the total voltammetric charge (Q*) as a function of IrO_2 loading.

These results differ with those reported by Savinell *et al.* [33] who found a continuous and linear increase of the voltammetric charge Q* with the electrochemically active surface area (the IrO_2 loading). In their experiments, they investigated IrO_2 films formed at the surface of titanium plates obtained by thermal decomposition of a precursor salt (H_2IrCl_6), over a large range of catalyst loading (from 0.88 to 2.7 mg cm^{-2}, see Figure 8-a and 8-b). One of the main difference between the two sets of experiments lies in operation conditions. The electrodes studied by Savinell *et al.* [33] were characterized in a liquid aqueous electrolyte (1 M H_2SO_4). In this case, it can be expected that all catalytic sites (including those located inside surface cracks) are probed. Regarding the results reported here, IrO_2 anodes were made of catalyst powder – ionomer mixtures in contact with a solid electrolyte. SEM micrographs of figure 1 suggest that anodes are made of densely packed layers of electronically conductive catalyst spheres. Voids and cavities are filled with ion-conducting ionomer. Hence the saturation of the voltamperometric charge observed at high catalyst loadings (Figure 5) can be explained by a lack of access of protons to catalytic sites located at the surface of particles embedded deep inside the electrode, away from the membrane surface, close to the backing Ti current collector.

In order to account for the experimental data of Figure 5, a simple geometric model has been used. In this model, the anode is represented by the stacking of successive layers of spherical catalyst particles (Figure 6). Underlying assumptions of the model are:

- electrochemically active sites of the first catalyst layer (in direct contact with the bulk membrane) are all accessible to protons; the full specific surface area ECSA of this first layer of particles is therefore:

  $$ECSA = \frac{6}{\rho D_{particle}}(1-\varepsilon) \qquad \text{Equation 2}$$

  where $D_{particle}$ is the particle diameter, ρ the volumetric weight of the particle material and ε is the pore fraction (ε= 0.33 in a cubic packing [33]*);*
- to access the next layers, protons are transported to/from the bulk membrane through ionomer pathways located along the porosities of the different layers. Since the catalyst layer is a mixture of catalyst particles and ionomer chains, the probability that a catalytic site of a given layer is not connected to the membrane increases layer after layer. Models developed for porous electrodes in liquid electrolytes take into account the fact that the wetting of the deep sites is limited by the porosity and tortuosity of the electrode. The same idea was used here. Accessible active sites in a given layer depend on the number of layers located up to the membrane. This is equivalent to a

kind of “shadow effect”. Hence, the electrochemically active surface area of individual layers in this stacking of catalyst particles depends on the cumulated shadow effects of other layers.

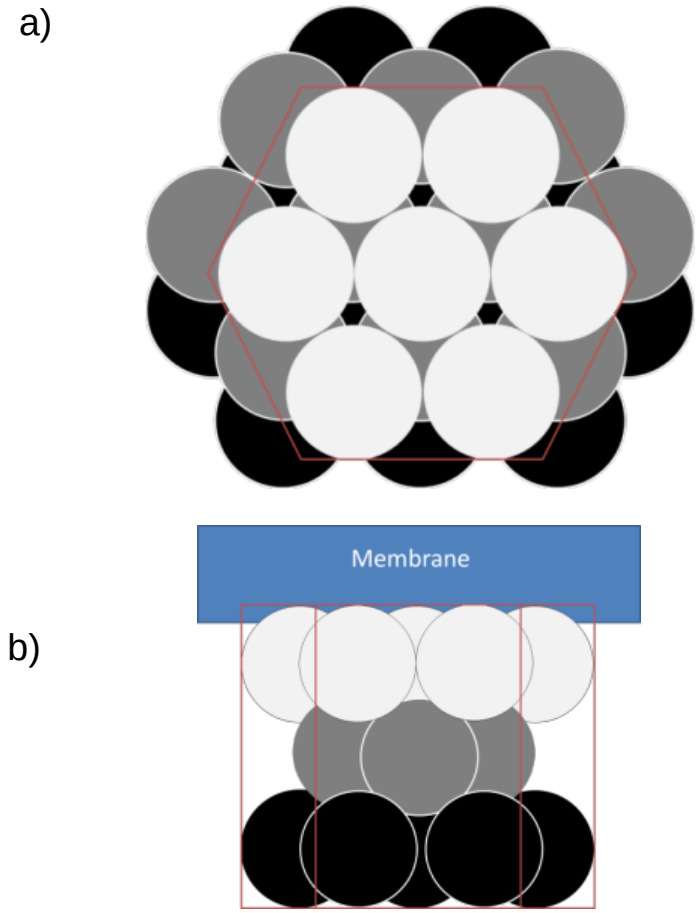

Figure 6: hexagonal close packing of IrO_2 spherical nanoparticles in the catalyst layer.

a) top view, b) side view.

The theoretical coulombic charge Q* of the anode is calculated by summing up the contribution of the N single layers of spheres, starting from the first layer in direct contact with the bulk membrane (light grey spheres in Figure 6) up to the last one in contact with the backing titanium current collector. As discussed before, the idea is that the contribution of each layer to Q* decreases with N: the contribution of the n^{th} layer to Q* is less than the contribution of the $(n-1)^{th}$ layer. Due to the complex geometry of the system, Q* has been calculated empirically using Equation (3):

$$Q^* = B \times \sum_1^N \exp\left(\frac{-n}{A}\right) \qquad \text{Equation 3}$$

Q* is the total voltammetric charge of the anode in C cm^{-2}.

B is a characteristic of the catalyst used at the anode; this is the coulombic charge in C cm^{-2} of the first layer of spheres in direct contact with the membrane (Eq. 2), which is close to the charge that could be measured on a flat surface.

n is the n^{th} layer of catalyst particles in the stack of N layers

The contribution of successive layers to Q* is postulated to decrease exponentially along the distance normal to the membrane, in order to account for experimental observations. This exponential distribution of catalytic sites along the thickness of the electrode is used to account for several physical parameter such as the ionomer content, porosity and tortuosity of conduction path within the anode that restrain the access of protons to the catalytic sites.

A is an empirical parameter that is used to set how the contributions of the N layers to Q* do vary. This is a floating parameter used to fit experimental data. The reference value (100%) indicates that the charge of the layer is equal to B (the charge of a flat surface). Subsequent layers contribute to Q* by only a fraction of B. Figure 7 shows a plot of the contribution (in %) of each layer, for different empirical values of A. When A is large (tends to infinity), the electrochemically active surface area of the particle of each single layer remains the same. In that case, each particle of any single layer is fully accessible to protons and the voltammetric charge increases linearly with the catalyst loading – as reported by Savinell*et al.* [33]. If A is low, this means that only the few first single layers are electrochemically active. Q* tends to a limit when the loading is increased, as experimentally observed.

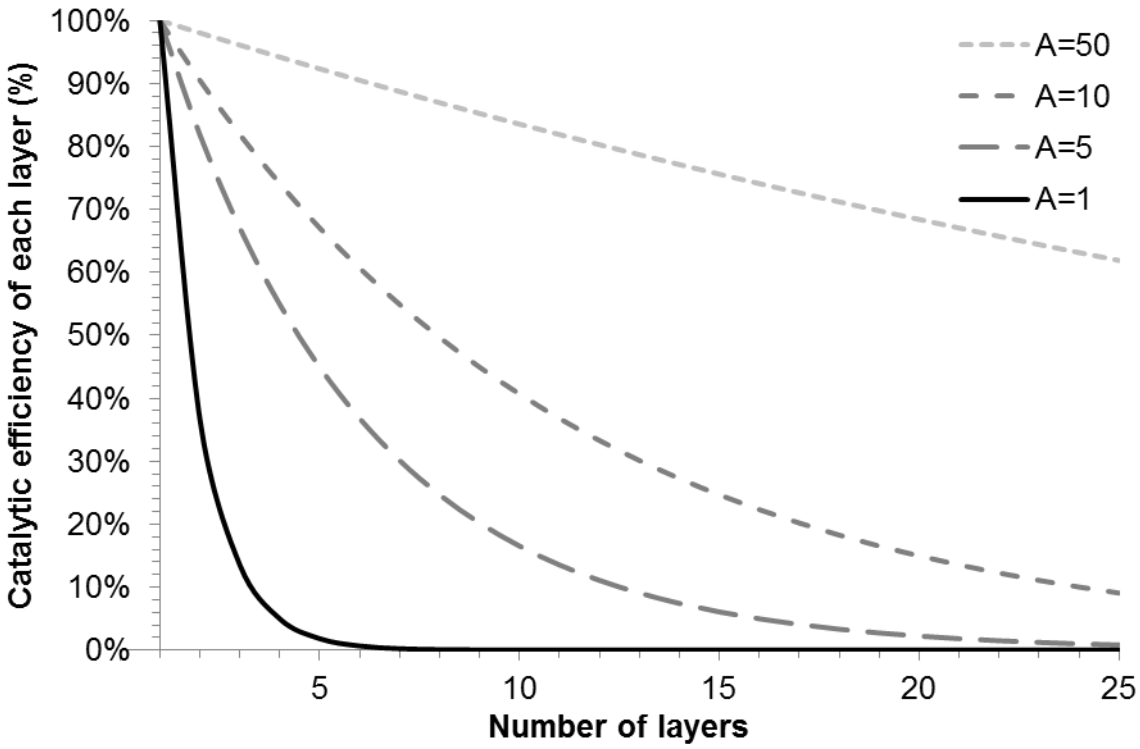

Figure7: Influence of the parameter A on the catalytic efficiency of each single layer in the stack of catalyst layers (ratio between the average electrochemically active surface area of the considered particle layer and the value assuming that the surface area is fully accessible to protons)

Let's now express Eq. (3) as a function of the shape of catalyst particles. Eq. (3) can be rewritten as:

$$Q^* = B \times \exp\left(-\frac{1}{A}\right)\frac{1-\exp\left(-\frac{N}{A}\right)}{1-\exp\left(-\frac{1}{A}\right)} \qquad \text{Equation 4}$$

The number of catalyst single layers "N" is related to the catalyst loading. Assuming that catalyst particles are spherical in shape (radius R), the mass of an individual iridium oxide nanoparticle is:

$$m_{particle} = \frac{4}{3}\pi\rho R^3 \quad \text{(g)} \qquad \text{Equation 5}$$

where ρ is the volumetric weight of iridium dioxide (ρ = 11.66 10^6 g m^{-3} [38]).

Assuming that catalyst spheres are packed in a simple hexagonal close packing structure, the density of circle packing in the plane is $\frac{\pi}{2\sqrt{3}}$. Hence, the weight of particles per single layer contained per unit surface is:

$$m_{layer} = \left(\frac{\frac{\pi}{2\sqrt{3}}}{\pi R^2}\right) \times \frac{4}{3}\pi\rho R^3 = \frac{2\pi}{3\sqrt{3}}\rho\mathrm{R}\ (\mathrm{g.m^{-2}})$$ Equation 6

Knowing the catalyst loading of the electrodes m_{IrO2} (in g m^{-2}), it is possible to calculate the number of single layers N contained in the electrodes:

$$N = \frac{m_{IrO_2}}{m_{layer}} = \frac{m_{IrO_2}}{\frac{2\pi}{3\sqrt{3}}\rho\mathrm{R}} = C \times \frac{m_{IrO_2}}{\mathrm{R}}$$ Equation 7

where $C = \frac{3\sqrt{3}}{2\pi\rho}$ Equation 8

In Eq. (8), C is a geometrical constant that can be used to consider different sphere packing (cubic, hexagonal, tetrahedral etc…).

Finally, Q* is given by:

$$Q^* = B \times \exp\left(-\frac{1}{A}\right)\frac{1-\exp\left(-C\frac{m_{IrO_2}}{\mathrm{R}\,A}\right)}{1-\exp\left(-\frac{1}{A}\right)}$$ Equation 8

Using equation 8, only two independent parameters (A and B) are required to fit the experimental plots of the total charge (Q*) versus the catalyst loading. Experimental data of figure 6 have been fitted using equation 8. Best fits were obtained with A = 86 and B =125 C m^{-2}. The same model and fitting procedure were then used to analyze data previously reported in the literature using dimensionally stable anodes prepared at 400°C by thermal decomposition of $IrCl_3$ salt on titanium plate [39], H_2IrCl_6 at 450 °C on titanium plate (average particle size: 51 nm diameter) [33] and H_2IrCl_6 at 500 °C on p-Si substrate in air [40]. Fits are plotted in Figure 8 and fit parameters are compiled in Table 1.

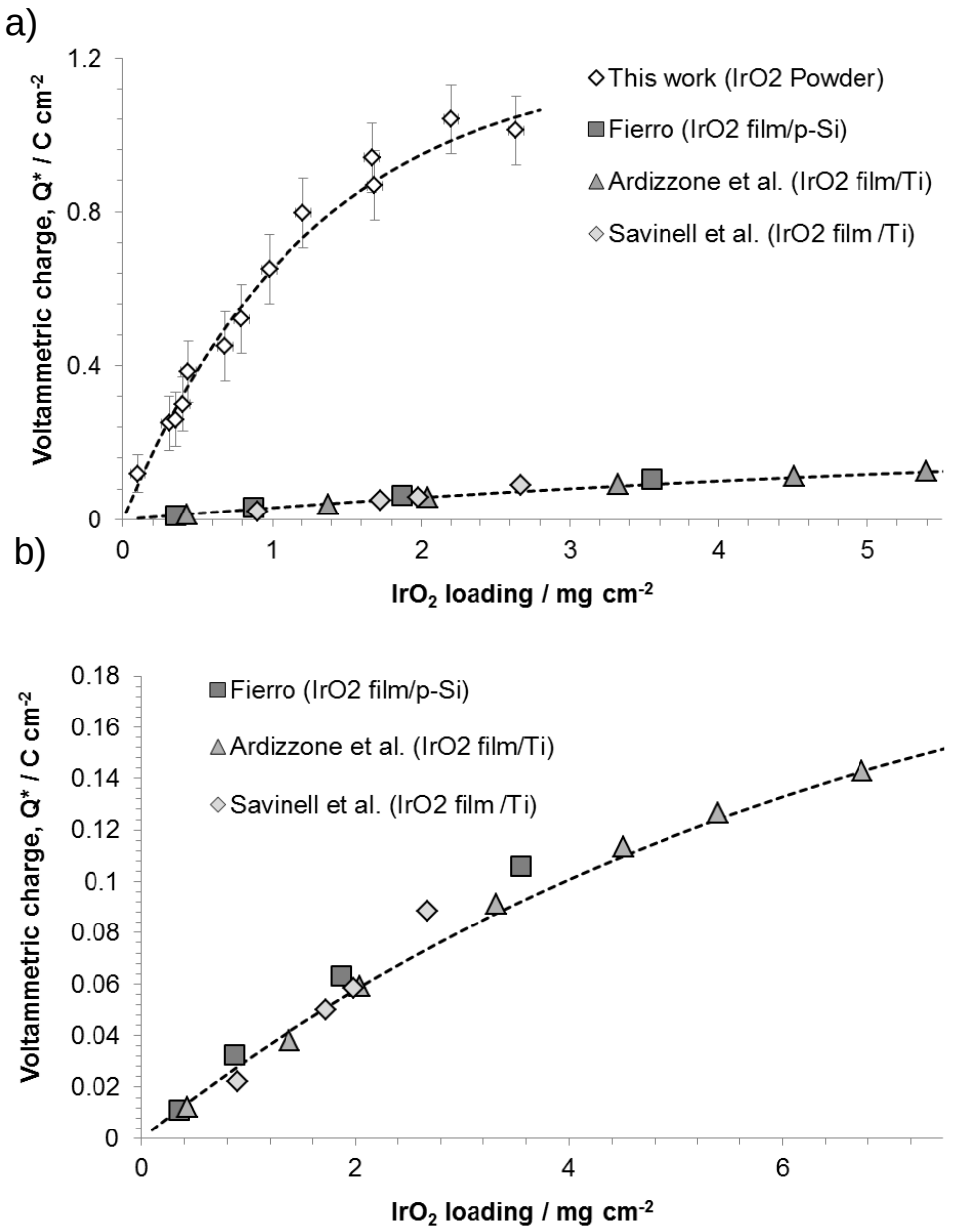

Figure 8: Voltammetric charge (Q^*) versus IrO_2 loading. a) Comparison of values measured on nanoparticle – based electrode (this work) with values on IrO_2 films prepared by thermal decomposition and reported by Fierro [40], Ardizzone *et al.*[39] and Savinell *et al.*[33]. b) zoom on the results reported in the literature and obtained by thermal decomposition of iridium chemical precursors.

Reference	Preparation method	A (a.u.)	B (Cm^{-2})
IrO_2PEMWE electrode (this work)	Nanoparticles	86	125
[39]	IrO_2 film formed on titanium plate by thermal decomposition of $IrCl_3$ salt at 400°C	190	12
[33]	IrO_2 film formed on titanium plate by thermal decomposition of H_2IrCl_6 at 450 °C		
[40]	IrO_2 film prepared by thermal decomposition H_2IrCl_6on p-Si substrate in air at 500°C		

Table 1: Parameters A and B derived from the simulation of voltammetric charge vs. IrO_2 loading curve.

The value of A obtained from the best fits for the nanoparticles – based electrodes (this work) half what was obtained with the thermally prepared IrO_2 films.This is an indication that deeply embedded catalytic sites on electrodes prepared by thermal decomposition of precursors are still active whereas those of nanoparticles electrode are not. Two explanations can be put forward to account for these results. First, Q* values obtained on IrO_2 electrodes prepared by thermal decomposition were measured in liquid electrolyte (1 M H_2SO_4 [33], 0.5 M [39], 1M $HClO_4$ [40]). Access of the protons to catalyst particles and sites in the electrolyte-filled porous structure is higher than in the case of porous catalyst – ionomer mixture filled with nonconductive de-ionized water. Second, the particles of IrO_2 electrodes prepared by thermal decomposition (mean diameter = 51 nm) are larger in size than those of the powder nanoparticles (15 nm). Electrodes porosity is higher when larger particles are used. Thus, catalytic sites are more accessible in these mesoporous structures (containing pores with diameters between 2 and 50 nm) than when nanoparticles are used. In addition, electrodes produced by thermal decomposition of precursor salts showed a higher number of large cracks that also contribute to increase the porosity of the electrodes. Regarding parameter B (the voltammetric charge of single layer of catalyst particles), the value obtained on IrO_2 nanoparticles is one order of magnitude higher than what is obtained on thermally prepared IrO_2 films. This is probably related to the larger specific surface area of the nanoparticles.

In conclusion, the voltammetric charge measured on the electrode containing IrO_2 nanoparticles is much higher than the charge measured on thermally prepared IrO_2 films. Considering the voltammetric charge only, the optimum loading of IrO_2 nanoparticles should be in the 1.5 - 2 mg cm^{-2} range.

3.3 PEM water electrolysis performances

The electrochemical performances of MEAs containing various anodic catalyst loadings were measured at current densities up to 2 A cm^{-2}. As reported in previous publications [8,41], the overvoltage of the OER is the major contribution to cell losses (the cathode exhibits good kinetics in this range of current densities). Typical polarization curves recorded at 80 °C with different IrO_2 loadings are shown in Figure 9. The general trend is that best performances are obtained with larger IrO_2 loadings.

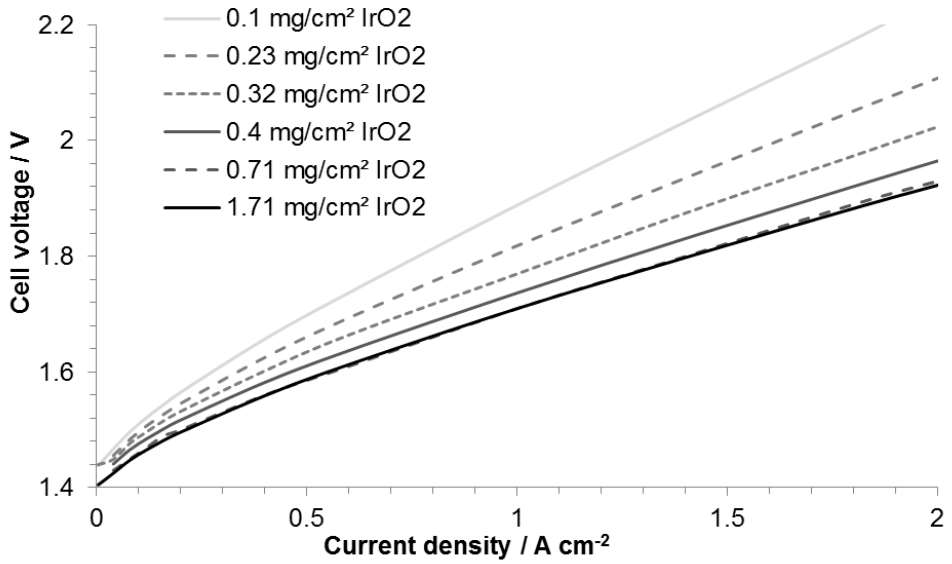

Figure 9: Polarization curves at 80°C using different anode catalyst loadings and 0.25 mg cm^{-2} Pt/C, and Nafion® 115 electrolyte membrane.

A plot of the cell voltage measured at 0.12 A cm^{-2} as a function of the anodic catalyst loading is provided in Figure 10. This plot shows the influence of anodic loading on charge transfer kinetics (at this low current density, the ohmic voltage drop due to the resistances of the cell and the membrane are small and can be neglected; hence results reflect the performance of anodes only). The cell voltage gradually decreases as the anodic loading increases until a value of approximately 1 mg cm^{-2} IrO_2 is reached. For larger loadings, the cell voltage remains constant. This decrease in cell voltage is due to the improvement of the kinetics of the OER which is directly related to the number of active sites (active surface area) available for the reaction. This trend is consistent with the evolution of the voltammetric charge Q* as a function of catalyst loading (Figure 5). The maximum activity of anodes is thus obtained for IrO_2 loadings of ≈1 mg cm^{-2} IrO_2.

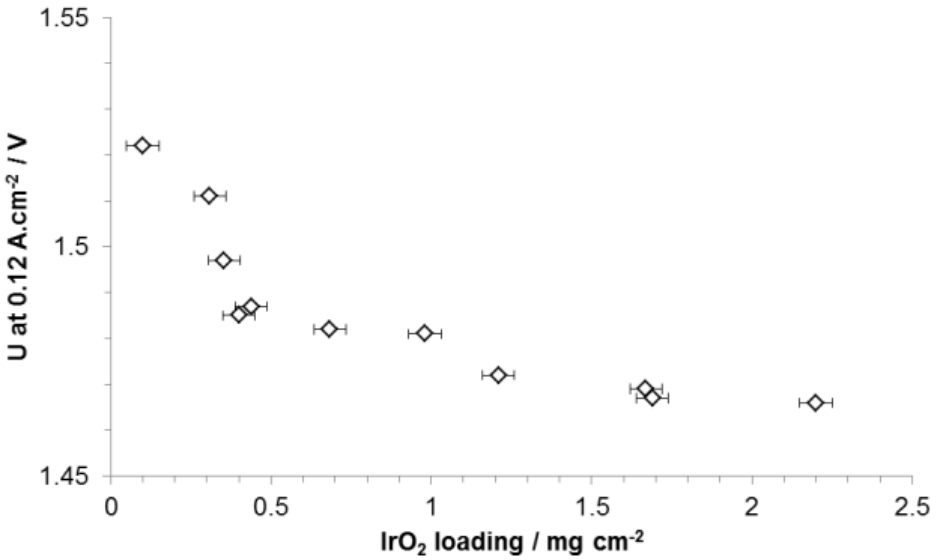

Figure 10: cell voltage at low current density (0.12 A cm^{-2}) as a function of anodic catalyst loading at 80°C.

A similar plot obtained at 1 A cm^{-2} is provided in Figure 11. In contrast to the results obtained at 0.12 A cm^{-2}, at this current density cell voltages are affected by ohmic cell resistances. Data give an indication on the electronic conductivity of the electrodes and on the contact resistance between electrodes and backing porous current collectors. A cell voltage of approximately 1.72 V is obtained at 1 A cm^{-2} and 80 °C for IrO_2 loadings up to 0.5 mg cm^{-2}. In the 0.5-2.6 mg cm^{-2} range, the electrode becomes thicker (see Figure 2). This results in an increase of the ohmic resistance of the cells due to the transport of protons through the catalyst layer, as already reported [9]. This increase of the ionic transport resistance counter-balances the positive effects due to the presence of a larger number of catalytic sites. It should be noted here that charge transfer resistances measured at low frequencies are not significantly affected by IrO_2 loadings. They only slightly increased at very low catalyst loadings (less than 0.3 mg cm^{-2}). According to Figure 11, a loading of 0.5 mg cm^{-2} appears to be a threshold value below which the performances of the cell drop quickly with the loading. This value corresponds to the minimum amount of catalyst required to obtain a good electronic conduction with inactive layers (lack of percolation of iridium oxide particles in the plane of the electrode) and a good contact between electrodes and backing current collectors. Therefore, as highlighted in Figure 10, below this threshold value of 0.5 mg cm^{-2} IrO_2, a catalyst support is needed to maintain the same level of electrochemical performances.

These estimations are consistent with SEM observations made on MEAs after electrochemical testing. For anodes with low anodic loading (Figure1-b), the surface presents cracks and

thickness heterogeneities. The number of catalyst particles is not sufficient to support the release of oxygen; the consequences of this situation are:

• a loss of active surface resulting in an increase in cell voltage at low current density (see Figure 10).

• a reduced electrical contact between the electrodes and the backing current collector which in turn lead to an increase of the ohmic resistance and an increase of the cell voltage at high current density (Figure 11).

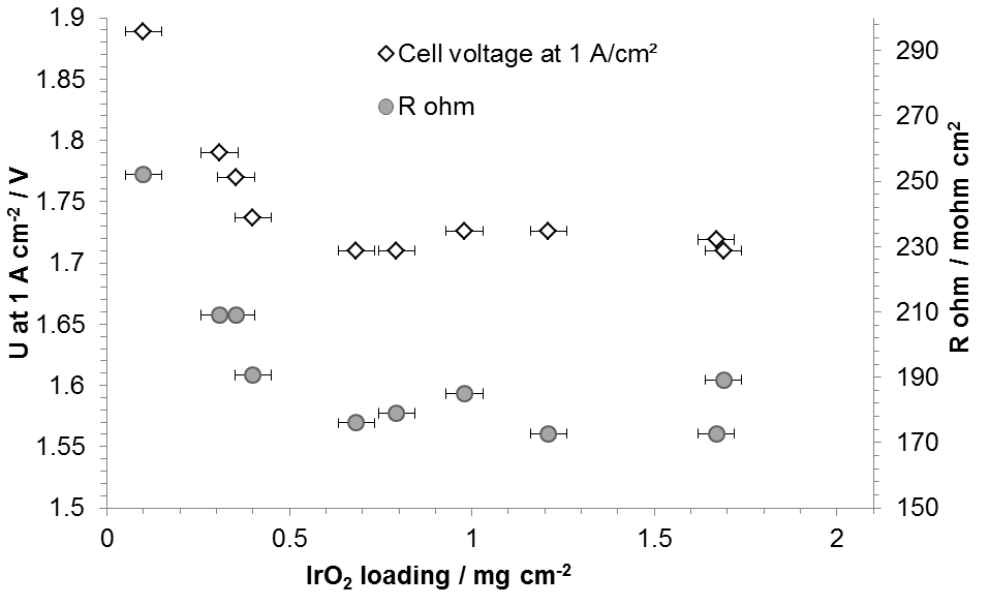

Figure 11: Cell voltage and ohmic resistance at high current density (1 A cm^{-2}) as a function of anodic catalyst loading at 80°C. Rohm corresponds to the total ohmic resistance in the cell including external circuit resistance, resistance of the electrodes and the electrolyte, and contact resistances.

4. Conclusions

The performances of PEM water electrolysis cells containing different IrO_2 loadings at the anode were measured and analyzed. A simple model is proposed to account for the relationship between the electric charge measured by cyclic voltamperometry (proportional to the number of electroactive sites) and the IrO_2 loading at the anode. Results show that a catalyst layer containing IrO_2 nanoparticles does not operate homogeneously. Active sites in volume are not involved in the OER mechanism. In terms of catalyst loading, electrochemical characterizations show that there is a threshold loading value of 0.5 mg cm^{-2} IrO_2 above which the cell voltage does no longer depend on catalyst loading (a cell voltage of 1.72 V was obtained with a Nafion® 115 membrane at 1 A cm^{-2}, 80°C and atmospheric pressure). Below this threshold, the percolation of individual iridium oxide particles becomes problematic and electrochemical performances tend to degrade rapidly. In this low loading range (< 0.5 mg cm^{-}

^{2} IrO_2), there is a need to add a conductive support of large surface area in order to keep a good conductivity inside the active layer and make all catalytic sites electrochemically active. A solution to this problem will be described in the second part of this research paper [42].

Acknowledgements

The authors want to acknowledge the financial support from the ANR (French National Research Agency) in the framework of the AITOILES project (ANR-11-PRGE-0001).

References

[1] F. Barbir, PEM electrolysis for production of hydrogen from renewables sources energies, Sol. Energy. 78 (2005) 661–669.

[2] E. Antolini, Carbon supports for low-temperature fuel cell catalysts, Appl. Catal. B Environ. 88 (2009) 1–24. doi:10.1016/j.apcatb.2008.09.030.

[3] S.A. Grigoriev, V.N. Fateev, H. Middleton, T.O. Saetre, P. Millet, A comparative evaluation of palladium and platinum nanoparticles as catalysts in proton exchange membrane electrochemical cells, Int. J. Nucl. Hydrog. Prod. Appl. 1 (2008) 343–354.

[4] S. a. Grigoriev, P. Millet, V.N. Fateev, Evaluation of carbon-supported Pt and Pd nanoparticles for the hydrogen evolution reaction in PEM water electrolysers, J. Power Sources. 177 (2008) 281–285. doi:10.1016/j.jpowsour.2007.11.072.

[5] S. a. Grigoriev, V.I. Porembskiy, S.V. Korobtsev, V.N. Fateev, F. Auprêtre, P. Millet, et al., High-pressure PEM water electrolysis and corresponding safety issues, Int. J. Hydrogen Energy. 36 (2011) 2721–2728. doi:10.1016/j.ijhydene.2010.03.058.

[6] J. Bard Allen, P. Roger, J. Joseph, Standard Potentials in Aqueous Solution, Monographs in Electroanalytical Chemistry and Electrochemistry, New York-B, 1985.

[7] P.N. Ross, The Corrosion of Carbon Black Anodes in Alkaline Electrolyte, J. Electrochem. Soc. 131 (1984) 1742. doi:10.1149/1.2115953.

[8] E. Rasten, G. Hagen, R. Tunold, Electrocatalysis in water electrolysis with solid polymer electrolyte, Electrochim. Acta. 48 (2003) 3945–3952. doi:10.1016/j.electacta.2003.04.001.

[9] L.R. Ma, S. Sui, Y.C. Zhai, Investigations on high performance proton exchange membrane water electrolyzer, Int. J. Hydrogen Energy. 34 (2009) 678–684. doi:DOI 10.1016/j.ijhydene.2008.11.022.

[10] J. Polonský, I.M.M. Petrushina, E. Christensen, K. Bouzek, C.B.B. Prag, J.E.T.E.T. Andersen, et al., Tantalum carbide as a novel support material for anode electrocatalysts in polymer electrolyte membrane water electrolysers, Int. J. Hydrogen Energy. 37 (2012) 2173–2181. doi:10.1016/j.ijhydene.2011.11.035.

[11] J. Polonský, P. Mazúr, M. Paidar, E. Christensen, K. Bouzek, Performance of a PEM water electrolyser using a TaC-supported iridium oxide electrocatalyst, Int. J. Hydrogen Energy. 39 (2014) 3072–3078. doi:10.1016/j.ijhydene.2013.12.085.

[12] S. Siracusano, V. Baglio, C. D'Urso, a. S. Aricò, Preparation and characterization of titanium suboxides as conductive support of IrO2 electrocatalysts for application in SPE electrolysers, Electrochim. Acta. 54 (2009) 6292–6299.

[13] A. Stoyanova, G. Borisov, E. Lefterova, E. Slavcheva, Oxygen evolution on Ebonex-supported Pt-based binary compounds in PEM water electrolysis, Int. J. Hydrogen Energy. 37 (2012) 16515–16521. doi:10.1016/j.ijhydene.2012.02.032.

[14] M. Miu, I. Kleps, M. Danila, T. Ignat, M. Simion, A. Bragaru, et al., Electrocatalytic activity of platinum nanoparticles supported on nanosilicon, in: Fuel Cells, 2010: pp. 259–269. doi:10.1002/fuce.200900202.

[15] R.E. Fuentes, J. Farrel, J.W. Weidner, Multimetallic electrocatalyst of Pt, Ru and Ir supported on anatase and rutile TiO2 for oxygen evolution in an acid environment, Electrochem. Solid State Lett. 14 (2011) E5–E7.

[16] P. Mazúr, J. Polonský, M. Paidar, K. Bouzek, Non-conductive TiO2 as the anode catalyst support for PEM water electrolysis, Int. J. Hydrogen Energy. 37 (2012) 12081–12088. doi:10.1016/j.ijhydene.2012.05.129.

[17] E. Mayousse, F. Maillard, F. Fouda-Onana, O. Sicardy, N. Guillet, 36 (17), 10474 – 10481, 2011, Int. J. Hydrogen Energy. 36 (2011).

[18] J. Xu, G. Liu, J. Li, X. Wang, The electrocatalytic properties of an IrO2/SnO2 catalyst using SnO2 as a support and an assisting reagent for the oxygen evolution reaction, Electrochim. Acta. 59 (2012) 105–112. doi:10.1016/j.electacta.2011.10.044.

[19] L. Vazquez-Gomez, S. Ferro, A. De Battisti, Preparation and characterization of RuO2-IrO2-SnO2 ternary mixtures for advanced electrochemical technology, Appl. Catal. B Environ. 67 (2006) 34–40. doi:10.1016/j.apcatb.2006.03.023.

[20] K. Kadakia, M.K. Datta, O.I. Velikokhatnyi, P. Jampani, S.K. Park, P. Saha, et al., Novel (Ir,Sn,Nb)O2 anode electrocatalysts with reduced noble metal content for PEM based water electrolysis, Int. J. Hydrogen Energy. 37 (2012) 3001–3013. doi:10.1016/j.ijhydene.2011.11.055.

[21] H.N. Nong, H.-S. Oh, T. Reier, E. Willinger, M.-G. Willinger, V. Petkov, et al., Oxide-Supported IrNiO x Core-Shell Particles as Efficient, Cost-Effective, and Stable Catalysts for Electrochemical Water Splitting, Angew. Chemie Int. Ed. (2015) n/a–n/a. doi:10.1002/anie.201411072.

[22] V.K. Puthiyapura, S. Pasupathi, H. Su, X. Liu, B. Pollet, K. Scott, Investigation of supported IrO2 as electrocatalyst for the oxygen evolution reaction in proton exchange membrane water electrolyser, Int. J. Hydrogen Energy. 39 (2014) 1905–1913. doi:10.1016/j.ijhydene.2013.11.056.

[23] V.K. Puthiyapura, M. Mamlouk, S. Pasupathi, B.G. Pollet, K. Scott, Physical and electrochemical evaluation of ATO supported IrO2 catalyst for proton exchange membrane water electrolyser, J. Power Sources. 269 (2014) 451–460. doi:10.1016/j.jpowsour.2014.06.078.

[24] J. Xu, Q. Li, M.K. Hansen, E. Christensen, A.L. Tomás García, G. Liu, et al., Antimony doped tin oxides and their composites with tin pyrophosphates as catalyst supports for oxygen evolution reaction in proton exchange membrane water electrolysis, Int. J. Hydrogen Energy. 37 (2012) 18629–18640. doi:10.1016/j.ijhydene.2012.09.156.

[25] A. MARSHALL, S. SUNDE, M. TSYPKIN, R. TUNOLD, Performance of a PEM water electrolysis cell using IrxRuyTazO2IrxRuyTazO2 electrocatalysts for the oxygen evolution electrode, Int. J. Hydrogen Energy. 32 (2007) 2320–2324. doi:10.1016/j.ijhydene.2007.02.013.

[26] A.A. Gusev, E.G. Avvakumov, A.Z. Medvedev, A.I. Masliy, Ceramic electrodes based on magneli phases of titanium oxides, Sci. Sinter. 39 (2007) 51–57.

[27] H. Su, B.J. Bladergroen, V. Linkov, S. Pasupathi, S. Ji, Study of catalyst sprayed membrane under irradiation method to prepare high performance membrane electrode assemblies for solid polymer electrolyte water electrolysis, Int. J. Hydrogen Energy. 36 (2011) 15081–15088. doi:10.1016/j.ijhydene.2011.08.057.

[28] D. Sievert, H. Baumann, G.G. Scherer, S. Stucki, Second Symposium on Electrode Materials and Processes for Energy Conversion and Storage, in: S. Srinivasan, S. Wagner, H. Wroblowa (Eds.), ECS Proc. Vol. PV 87-12, Pennington, NJ USA, 1987: p. 367.

[29] H. Su, V. Linkov, B.J. Bladergroen, Membrane electrode assemblies with low noble metal loadings for hydrogen production from solid polymer electrolyte water electrolysis, Int. J. Hydrogen Energy. 38 (2013) 9601–9608. doi:10.1016/j.ijhydene.2013.05.099.

[30] B.-S. Lee, S.H. Ahn, H.-Y. Park, I. Choi, S.J. Yoo, H.-J. Kim, et al., Development of electrodeposited IrO2 electrodes as anodes in polymer electrolyte membrane water electrolysis, Appl. Catal. B Environ. 179 (2015) 285–291. doi:10.1016/j.apcatb.2015.05.027.

[31] B. Bladergroen, H. Su, S. Pasupathi, V. Linkov, Overview of Membrane Electrode Assembly Preparation Methods for Solid Polymer Electrolyte Electrolyzer, in: Electrolysis, 2012: pp. 45–60. doi:10.5772/52947.

[32] M. Carmo, D.L. Fritz, J. Mergel, D. Stolten, A comprehensive review on PEM water electrolysis, Int. J. Hydrogen Energy. 38 (2013) 4901–4934. doi:10.1016/j.ijhydene.2013.01.151.

[33] R.F. Savinell, R.L.Z. Iii, J.A. Adams, R.L. Zeller Iii, J.A. Adams, Electrochemically Active Surface Area Voltammetric Charge Correlations for Ruthenium and Iridium Dioxide Electrodes, J. Electrochem. Soc. 137 (1990) 1–6.

[34] A. Marshall, Electrocatalysts for the Oxygen Evolution Electrode in Water Electrolysers using Proton Exchange Membranes : Synthesis and Characterisation, PhD Thesis, Norwegian University of Science and Technology, 2005. http://ntnu.diva-portal.org/smash/get/diva2:126008/FULLTEXT01.pdf.

[35] S. Trasatti, G. Buzzanca, Ruthenium dioxide: a new interesting electrode material. Solid structure and electrochemical behaviour, J. Electroanal. Chem. Interfacial Electrochem. 29 (1971) A1–A5. doi:10.1016/S0022-0728(71)80111-0.

[36] S. Ardizzone, G. Fregonara, S. Trasatti, “Inner” and “outer” active surface of RuO2 electrodes, Electrochim. Acta. 35 (1990) 263–267. doi:10.1016/0013-4686(90)85068-X.

[37] G. Lodi, E. Sivieri, A. Debattisti, S. Trasatti, Ruthenium Dioxide-Based Film Electrodes .3. Effect of Chemical Composition and Surface Morphology on Oxygen Evolution in Acid-Solutions, J. Appl. Electrochem. 8 (1978) 135–143. doi:10.1007/bf00617671.

[38] M.L. Williams, CRC Handbook of Chemistry and Physics, 76th edition, Occup. Environ. Med. 53 (1996) 504. doi:10.1136/oem.53.7.504.

[39] S. Ardizzone, A. Carugati, S. Trasatti, Properties of thermally prepared iridium oxide electrodes, J. Electroanal. Chem. 126 (1981) 287–292. doi:10.1016/S0022-0728(81)80437-8.

[40] S. Fierro, Electrocatalysis Induced by Surface Redox Activities on Conductive Metal Oxide Electrodes; PhD Thesis, Ecole Poytechnique Fédérale de Lausanne, 2010. http://infoscience.epfl.ch/record/142943/files/EPFL_TH4619.pdf.

[41] E. Rasten, Electrocatalysis in water electrolysis with solid polymer electrolyte, PhD Thesis, Norwegian University of Science and Technology, 2001. http://www.diva-portal.org/smash/get/diva2:121826/FULLTEXT01.pdf (accessed February 1, 2013).

[42] C. Rozain, E. Mayousse, N. Guillet, P. Millet, Influence of iridium oxide loadings on the performance of PEM water electrolysis cells: Part II – Advanced oxygen electrodes, Applied Catalysis B: Environmental, submitted.